Heliyon 10 (2024) e26051

Contents lists available at ScienceDirect

Heliyon

journal homepage: www.cell.com/heliyon

Review article

Electrodeposited carbon nanostructured nickel composite coatings: A review

Shikha Awasthi [*], Suranjan De [***], Sarvesh Kumar Pandey [**]

Department of Chemistry, Manipal University, Jaipur, India

ARTICLE INFO

Keywords:
Nickel
Carbon
Nanoallotropes
Mechanical
Aerospace

ABSTRACT

The utilization of high-strength materials that can retain their strength after successive use under high mineral moisture (maximum weight of 1098 kg) for aerospace, automotive, and electromagnetic devices is challenging. Generally, coatings of nickel (Ni) and its alloys are utilized in the aforementioned applications, but the continuous use of the system degrades its mechanical stability and structural integrity. For the automotive and aerospace uses, the material should have high mechanical strength, wear tolerance, corrosion resistance, and magnetism. The bare Ni coatings can be altered with enhanced mechanical, tribological and electrochemical performances by using various reinforcements in the coatings. The abundantly used reinforcing agents are mainly carbonaceous nanoallotropes (such as graphene, carbon nanotubes, and diamond) for the fabrication of composite coatings. The current review unfolds the introduction of nickel and the major cause of damage to bare nickel coatings. Moreover, the review sheds light on how to mitigate the damage of nickel coatings with an emphasis on giving a flavor of distinct carbonaceous nanoallotropes. The conjugated studies on mechanical, wear, corrosion, and magnetic behavior of electrodeposited Ni-carbonaceous composite coatings are embraced in the review. Therefore, the present review can be endorsed by the readers for the protection of aircraft, automotive, and electromagnetic appliances.

1. Introduction

The applications of nickel coatings are in majorly aerospace or automotive industries (~33 %), metal fabrication and electrical equipment (~13–20 %), electromagnetic devices, supercapacitors, petroleum and chemical industries (Fig. 1, ~5–7 %) [1–3]. Ni is low-cost, easily obtainable, affluent on earth, and environmentally amiable which has an important component of enzyme active centers, it performs a critical function, notably in the field of organismal biochemistry.

Nickel is a key ingredient in the aerospace industry, particularly in the manufacture of aircraft components such as the nose cone, engine cowlings, edge flaps, and stabilizers (see Fig. 2). Nonetheless, nickel is used in a variety of applications, most notably wheels, pinion shafts, slip yokes, carburetor fuel connections, relays, motors, and pumps in the automobile industry, as well as electromagnetic appliances [5]. Innovative aviation scientists have chosen to substitute standard stainless-steel alloys with sophisticated nickel alloys, notably in turbines, specifically within the combustion chamber. In the modern day, a single jet engine contains around 1.8 tons of

* Corresponding author.
** Corresponding author.
*** Corresponding author
E-mail addresses: suranjan.de@jaipur.manipal.edu (S. De), skpchmiitk@gmail.com (S.K. Pandey).

https://doi.org/10.1016/j.heliyon.2024.e26051
Received 13 September 2023; Received in revised form 7 February 2024; Accepted 7 February 2024
Available online 16 February 2024

nickel alloys, a game-changing addition that allows for approximately 20,000 flying hours without significant maintenance. This is in sharp contrast to the old benchmark of a 5-h flight length prior to the adoption of nickel alloys as a regular practice. Clearly, this transition has made nickel crucial in the aircraft sector, highlighting its significant influence on the development of aviation technology. Despite nickel in its pure form is resistant to corrosion, its wear efficiency is inadequate due to its poor hardness and tensile strength. Nickel alloying considerably improves its strength, durability to wear, and resilience to corrosion [6]. Large-scale industrial electrodeposition of nickel and Ni-based alloy coatings is a common approach for protecting various machine components from damaging external impacts. Enhancement of hardness, wear resistance, and corrosion resistance can be achieved by the inclusion of metals in these coatings with superior features. The hardness of the alloy coatings can be elevated due to the variation obtained in the microstructures and the composition of alloy [7]. As for example, microhardness and wear resistance in a pure nickel (Ni) matrix can be modulated by the addition of Boron (B). Due to the high abrasion and protective assets achieved in the Ni-B alloys, these are utilized in the field of aerospace, automotive, electronics, and the chemical industry [8]. Improvement in terms of corrosion resistance and tribomechanical functioning of electrodeposited Ni-Mo alloys can be attained by treatment with Cr_2O_3 nanoparticles. The formulated nanocomposite layers of Ni-Mo-Cr_2O_3 exhibited lower wear mass loss and coefficient of friction (COF) as compared to Ni-Mo alloy layer, irrespective of Cr_2O_3 nanoparticles loading. Using the Ni–Mo–Cr_2O_3 nanocomposite films coating on mild steel may increase the lifespan and durability of mild steel used in industrial purposes [9]. Hard particles, such as oxides, carbides, or diamonds, increase the mechanical assets of metal or alloy objects, making them ideal for a broad range of industrial usage. Additionally, the incorporation of ceramic components to the alloy matrix enhances the material's mechanical properties through changes in crystal and coating morphology [10]. TiC is a widely regarded ceramic material with enormous promise due to its remarkable physical and chemical characteristics. It possesses a significantly high melting point, outstanding hardness, superb antioxidation characteristics, and better chemical resistivity [11]. In addition to that, it has an outstanding immunity to corrosion and wear. TiC is becoming a more preferred reinforcing particle in composite coatings, according to recent trends, which has improved the mechanical, structural, and corrosion characteristics for a variety of applications [12–14].

The theory of Ni deposition was established by Calhane and Gammage [15] in 1907 using the method for the study of impurities in Ni deposition. Afterward, Ni deposition became a commercial and versatile protective coating process as approximately 100,000 metric tons of Ni is consumed worldwide in the form of metal and salts for electroplating [16]. Several fabrication techniques such as direct current deposition, pulse reverse current deposition, electroless plating, chemical vapour deposition, etc. have been used in order to process Ni coatings for the protection of the material's surface. Electroless Ni plating, processed by Ambat et al. [17] at 60 °C temperature for 250 min time, pH 7–8 and the hardness was reported to be 600–700 VHN. However, Maruyama et al. [18] fabricated Ni film by chemical vapour deposition using nickel acetylacetonate as raw material at a reaction temperature above 250 °C. The XRD pattern in Fig. 3 shows the cubic structure of Ni film with the composition of crystallites. Ni coating obtained at 270 °C (Fig. 3a) reaction temperature shows the prominent peak of (111) plane while above 300 °C (Fig. 3b) reaction temperature, this peak shows some deviation due to the thermal decomposition of nickel acetylacetonate in the vapour phase (Fig. 3).

Nonetheless, the deposition of Ni using direct current and pulsed current was carried out at 65 °C temperature for 75 min using Watts's bath [19]. The electrochemical testing exhibited an enhanced polarization resistance for pulsed current deposited Ni (8.06 KΩ) when compared to that of direct current deposited Ni (0.8 KΩ) [19]. Besides the several deposition techniques, in the present work, the pulsed electrodeposition process was employed for the fabrication of Ni composite coatings. The bare Ni coating can deteriorate after a short time of consumption of material in wear and corrosive conditions. A description of these depreciative factors is given below.

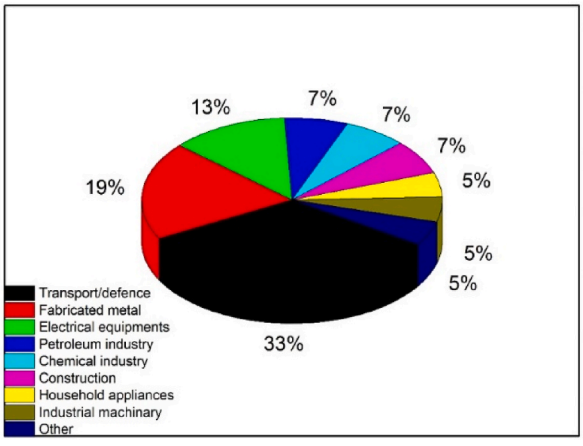

Fig. 1. Ni in various fields of applications. Concept adapted and redrawn from ref. [4].

2. Failure of materials and their protection

2.1. Failure by corrosion and wear

Environmental factors (chemical reaction, humidity and temperature), stress (compression and shear), manufacturing defects and constant loading-unloading are the main factors that can cause corrosion, wear and fatigue failure in the materials.

Corrosion is the natural process through which a pure metal converts to a state with greater stability such as oxide, hydroxide, or sulphide. The predominant kinds of corrosion include galvanic corrosion, localized corrosion, uniform corrosion, intergranular corrosion and high-temperature corrosion. Galvanic corrosion occurs when two distinct metals (cathode and anode) are exposed in an electrolyte under the influence of an electric field while localized corrosion affects only a specific area of the metal and comes in three varieties pitting, crevice, and filiform corrosion. Pitting corrosion occurs when a tiny hole or cavity appears in the metal, causing this region to become anodic while the remainder of the metal serves as a cathode. Nevertheless, acidic environments or a lack of oxygen in the crevice cause corrosion in crevices. Filiform corrosion develops whenever water penetrates a painted or plated surface, beginning with a minor fault in the coating and spreading to cause structural damage. Uniform corrosion arises through chemical or electrochemical processes and corrodes enormous amounts of metal to the point of utter breakdown, but it is controlled, foreseeable, and frequently preventive. Intergranular corrosion is a chemical or electrochemical attack on metallic particle borders caused by contaminants at the particle border whereas in high-temperature corrosion, vanadium sulfate-containing gas turbine and diesel engine fuels can generate low melting compounds during combustion, which are exceptionally corrosive to metallic alloys. Similar to corrosion, wear is a phenomenon that causes material deterioration. Wear is the deterioration of a material's outermost layer caused mostly by mechanical engagement with another opposing layer. The main types of wear are adhesive wear, abrasive wear, fretting wear and erosive and corrosive wear. Adhesive wear refers to the undesirable dislocation and attachment of wear debris from one surface to another surface during friction motion while abrasive wear occurs when a particular surface travels across a different one that is tougher. It is classified as two-body abrasive wear or three-body abrasive wear depending upon the type of surface that comes into contact. Fretting wear is a continual cycling rubbing of ~ 100 μm amplitude between two surfaces. Erosive wear occurs by the impact of solid or liquid particles against an object which can remove material from the surface through repeated deformation or cutting actions. On the other hand, corrosion wear (chemical or oxidation wear) is caused by the electrochemical or chemical reactions between metal and the environment [20]. The Prudhoe Bay oil leak of 2006 was the largest and most major accident in Prudhoe Bay's record. Corrosion inside the pipe caused the leak, which was caused by a quarter-inch hole that had formed at the transit pipeline's base. Nonetheless, the aircraft crash in Sweden in 1990 and the damage of aircraft Embraer 120, in Canada and Brazil, in 1994 are also cases of failure due to corrosion and wear. Exfoliation corrosion and intergranular attacks both have a negative influence on the durability of aeroplanes, cars, and numerous electromagnetic equipment. A notable example happened on July 25, 1990, while on a geological survey, culminating in the terrible death of an airplane pilot and crew. In one case, the right wing's outboard part split from their Aero Commander 680, resulting in a catastrophic crash in a Swedish field. Following examinations, it was discovered that pits from corrosion had damaged the wing's quality, permitting stress fractures to form in the lower spar cap [21]. Besides, several other cases of failure of different aircraft like Embraer 120, in Canada and Brazil, 1994 due to corrosion pitting and fatigue have been recognized as substantial safety hazards. Additionally, corrosion and wear can also damage the parts of a vehicle like the engine, engine bearings, piston assembly, etc. Improvement in wear and corrosion performance of these parts can generate several advantages of reduced fuel and oil consumption, improved engine power components, greater dependability, longevity, prolonged engine life, and reduced servicing needs throughout a long period [22]. Thus, the protection of these crucial components via protective coatings is critical.

Different scientific sectors are promoting the use of high-strength carbon-based additives such as graphite, diamond, carbon nanotubes (CNTs), carbon black, and buckminsterfullerene to meet strict safety, security, and efficiency standards [23]. Diamond, the sp^3 hybridized allotrope was first time synthesized as a thin film in 1988 and went on to be the Science magazine's molecule of the year. The C nanostructures approach with either 2D graphene or quasi-1D CNTs has remarkable significance in the miniaturization of electronics. Hence, the combination of Ni with carbonaceous reinforcements may achieve the potential requirements to mitigate the

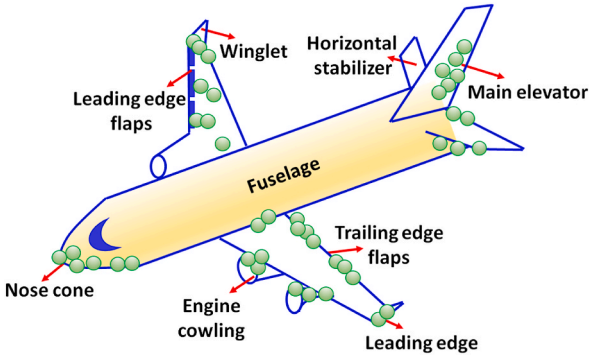

Fig. 2. Schematic showing the use of Ni coating in different parts of aircraft (marked by the circles).

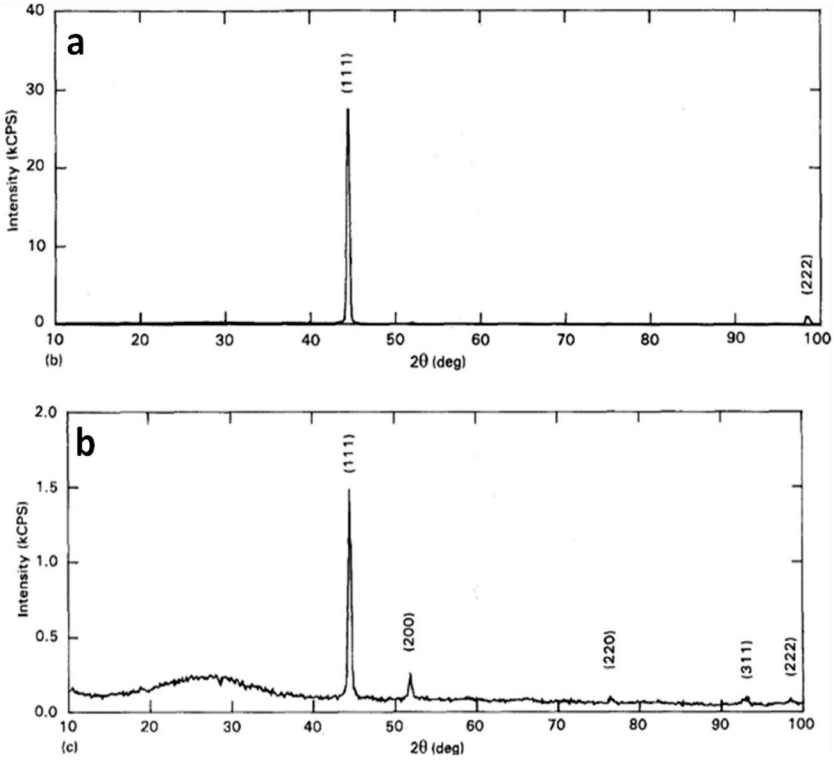

Fig. 3. XRD pattern of Ni film obtained at different reaction temperatures: (a) 270 °C and (b) 300 °C. Reproduced with permission from ref. [18].

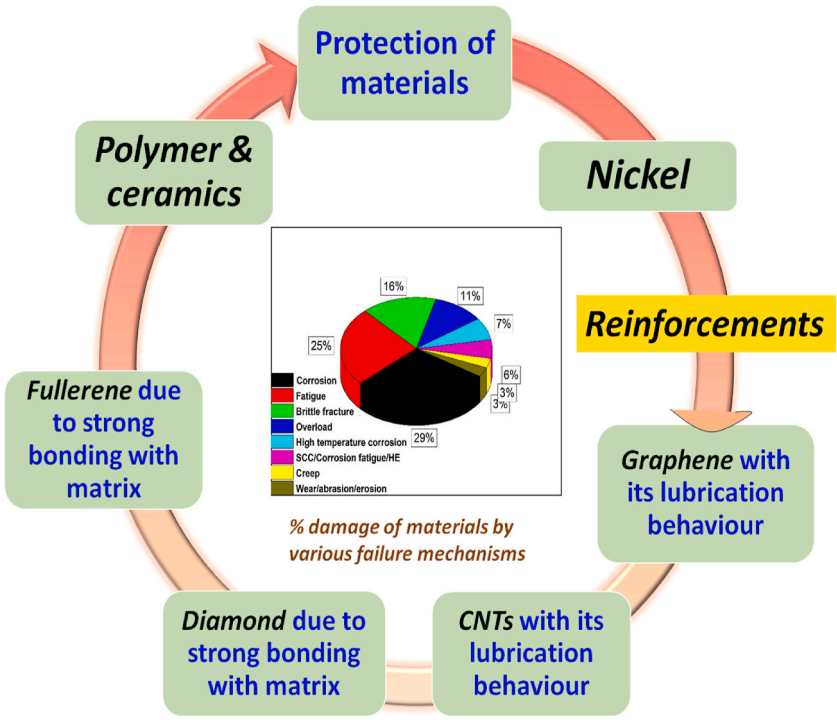

Fig. 4. Percentage damage of engineering components by various failure mechanisms along with the selective protective materials. Concept adapted and redrawn from ref. [4].

corrosion and wear of appliances. A short depiction of the mechanism of diamond, CNT, and graphene in order to protect the material is given below. Fig. 4 shows the total damage of engineering components due to various modes of failure along with the various protective components.

2.2. Protective materials from corrosion and wear

The carbonaceous reinforcements are the most auspicious candidates, utilized to reinforce the matrix as well as to protect materials from stress corrosion, and wear. The following is a summary of these allotropes.

2.2.1. Graphene reinforcements

Graphite is composed of a stable, layered, planar structure in which the individual layers are called graphene. The atoms of the carbon plane are bonded strongly via a covalent bond with only three of the four valence bonding sites. Graphene has a two-dimensional (2D) one-atom-thick planar sp^2-bonded carbon hexagonal nanosheet lattice structure which is arranged in a honeycomb crystal lattice and recently, it has been added to the carbon family as a new class of nascent carbon nanomaterials [24]. Because of the unconstrained mobility of its electron inside the lattice plane and weaker van der Waals associations between consecutive layers, graphene possesses a high conductivity. Graphene is useful in a variety of applications including carbon microphones, arc lamp electrodes, batteries, and dry lubrication [25]. Geim and Novoselov's discovery of graphene in 2004 was a watershed moment, winning them the Nobel Prize in Physics in 2010. This outstanding carbon nanomaterial generated a huge increase in graphene interest [26]. Graphene's structural stability is due to the densely packed arrangement of its carbon atoms, which are bonded by σ bonds. Graphene is nearly transparent and is about 200 times stronger than the strongest steel and it can efficiently conduct electricity and heat. As a result, graphene is emerging as a key substance in physics, chemistry, material science, and nanotechnology. Graphene acts as a zero-gap semiconductor because its conduction and valence bands coincide at the Dirac points. Because of its considerable surface area and excellent conductivity, graphene has received a lot of curiosity in the realm of electrochemical devices.

2.2.2. Carbon nanotubes (CNT) reinforcements

Carbon nanotubes is discovered by Iijima [27], which provided a great contribution to the broad range of applications related to biomedical, nanotechnology, environmental, robotics, domestic, etc. CNTs have an unusual hollow geometry, linked with conjugated all-carbon atoms involved in their structure. Given that nanotubes are representatives of the fullerene structural family, carbon nanotubes (CNTs) are made up of concentric carbon hexagons with both ends commonly enclosed by pentagons. CNTs. Like graphite, they have a chemical structure that is entirely made up of sp^2 bonds. Because of their mesoporous structure, they are often utilized as potent catalysts or catalytic aids for usage in energy-related sectors, as well as active electrodes in batteries, solar cells, fuel cells, and supercapacitors [28].

2.2.3. Diamond reinforcements

Diamond is a metastable allotrope of carbon which appears as a clear colourless crystal, and it is less stable than graphite. Every single carbon atom in a diamond is tetrahedrally (sp^3 hybridized) bonded to four other carbon atoms in a dense covalent network lattice in a regular repeated pattern, making it highly stiff (not very reactive). Diamond, for instance, is the hardest known natural material, with the maximum thermal conductivity (2200 W/m.k.) of any bulk solid. Based on those properties, it has major industrial interests especially polishing and cutting tools and also the scientific uses in diamond knives and diamond anvil cells. Notably, diamond has a wide band gap (5.5 eV) which falls in deep ultraviolet wavelength and also high optical dispersion. Diamonds have been adapted for many applications including distinctive thermal, mechanical, optoelectronic, and biological properties for various important applications. Nanodiamonds have unusual environmental stability and mechanical properties. In addition to that, Diamonds also offer numerous they possess several fascinating properties that include high thermal stability ($>250\ ^\circ C$), a high value of dielectric constant (3.5 K) and a reduced dissipation factor of 0.05 %. These interesting parameters of diamond make it an appealing alternative for a broad group of applications like field emission displays, clinical, hydrogen storage, microelectromechanical systems and electrochemical analysis [29].

2.2.4. Fullerene reinforcements

Buckminster fullerene shows a ball-like structure, and the smallest molecule is represented with a C60 configuration. The C60 molecule represents 12 pentagons and 20 hexagons and was discovered by Kroto et al., in 1985 [30]. This discovery has created an entirely hot topic and a new branch in the field of carbon chemistry, and its usefulness was admitted by Nobel Prize winner Baum in chemistry in 1996. The fullerene molecule has an architecture comparable to graphite, which is made up of layered graphene sheets with linked hexagonal rings. Due to the angle strain created by the bending shape of the closed sphere, fullerenes are resilient but not completely non-reactive. This peculiar hollow, football-like structure of fullerene C60 and its derivatives has been the subject of rigorous study, both for their technological innovations such as superconductivity, magnetic, and photonic assets, as well as biomedical applications. Moreover, their unique chemistry, particularly in the fields of electronics, nanotechnology, and material science, is of great interest to the scientific community [31]. Thus, the blending of these magical carbonaceous nanoallotropes with nickel matrix can alter the mechanical, tribological, electrochemical, and magnetic performance of bare nickel significantly. The description of recent studies related to Ni-carbon composite coatings can give a spectacular overview to the readers for the deliberation of perfect future research based on nickel and carbonaceous nanoallotropes.

3. Applications of carbonaceous materials

Ni has applications for decorative or engineering purposes. Decorative bright Ni can be used for exhaust pipes, trim, rims, hand tools, household appliances, etc. The major applications for various carbonaceous materials are described in consecutive sections.

3.1. Applications of graphene

Field emission is the release of electrons from a surface caused by the presence of a strong electric field. This method is useful for a variety of technical purposes, including adjustable X-ray producers and coiled field emission displays. Graphene cathodes have been designed particularly for field emission. These cathodes have an ohmic connection, requiring just a 1 V/μm electric field to initiate electron emission. These features, together with a high field enhancement factor of 7500 and a current density of 14 mA/cm^2, make them ideal for use in field emission technologies [32]. Due to the high surface area and conductivity, graphene can be used as sensors for the purpose of electrodes for heart rate monitoring, H_2O_2 sensors, strain sensors, NO_2 gas sensors, acetone and methanol sensors and glucose sensors [33]. Schedin et al., in 2007 [34], reported the first time the graphene-based sensors in which graphene demonstrated as a good sensor for NH_3, H_2O, NO_2 and CO. Graphene-based field effect transistors were first reported by Novoselov et al. [35] revealed graphene-based field effect transistors for the first time in 2004, observing an ambipolar a hallmark with an electron and hole concentration of 1013 sq-cm and mobilities up to 10,000 sq-cm/V-s at room temperature, as well as ballistic transport up to sub-micrometre distances. For transistor uses, graphene ought to appear in the form of graphene nanoribbons with a quasi-1D structure, limited width, clean edges, and a band gap with excellent carrier mobility. Organic light-emitting diodes (OLED) are utilized in gadget displays where minimal energy consumption is required. Therefore, the use of graphene as a substitute for indium in flat panels of OLED and mobile phones saves costs while also eliminating the demand for metal, which benefits gadget reuse and recycling [36]. Because of its unique capacity and reversible character, graphite is commonly used as an anode in Li-ion batteries. However, as the need for Li-ion batteries grows, graphene appears as an anode material with excellent stability, capacity, tolerance, specific area, and electrical conductivity [37]. Graphene irregularities are responsible for the attachment of Li ions to the anode with a faster charging time than traditional lithium-ion battery cells.

3.2. Applications of carbon nanotubes

EPD CNT coatings are ideal choices for field emission gadgets due to their chemical and thermal resistance, large aspect ratio, and tiny size, which contribute to high emission current densities while maintaining a low emission threshold. CNTs exhibited an emission current of 35 μA at an anode voltage of 1000 V and gate voltage of 60 V [50]. The superior motion imagery efficiency and energy economy of CNTs field emission displays allow them to be ideal candidates for a variety of applications, including cathode ray tubes, flat panel displays, and backlights for liquid crystal displays. The electrophoretic deposition (EPD) of CNTs offers an enormous benefit in the field of fuel cell usage (see Table 2). This benefit comes from the ability to control the catalyst and level of carbon by changing the current and deposition time. Thus, EPD CNTs are suitable for membrane electrode assemblies for fuel cells [51]. The sequential form of CNTs offered a much more advanced fuel cell than a disordered form of CNTs due to the higher electronic conductivity of CNT at its axis and high gas permeability with ordered CNTs with superhydrophobicity. A combination of CNTs with transition metal oxide or conducting polymer is a suitable candidate for supercapacitors. The usage of CNTs increases energy storage capacities by granting mechanical stability, large surface area and low resistance [52]. CNTs with high mechanical strength, small size, flexibility and conductivity, can be exploited as nanoprobes and sensors for applications in drug delivery, field emission etc. [53]. CNT-based sensors have faster response time than polymer or solid-state sensors. The strong capillary forces of CNT make it a capable candidate to hold fluids and gases inside them and thus can be employed as templates [54]. Marine current turbines should have sufficient strength to overcome challenges like dynamic effects, high flow velocity fluctuations in the ocean, cavitations, high bending forces etc. CNTs with high mechanical strength can be used as the filler for marine current turbines [55]. The mechanical properties and different resonance frequencies of CNTs can attributed to the tuned resonance mechanical frequency which has applications in several CNT-based tunable

Table 1
Mechanical properties: Hardness (H), elastic modulus (E) and fracture toughness (K_{IC}) of Ni-graphene, Ni-CNT and Ni-diamond with coatings temperature (T), pH and current density (I).

Coatings	EPD parameters	H	E (GPa)	K_{IC} (MPa)	References
Ni-graphene	T = 45 °C, pH 3–4 and I = 0.1 A/cm^2	610 HV	–	–	[38]
Ni-graphene	T = 50 °C, I = 0.15–4 A/dm^2	479 HV	240	–	[39]
Ni + graphite	T = 40 °C, pH 4, I = 8–10 A/dm^2	Tensile strength 345 MPa	–	–	[40]
Ni-CNT	T = 60 °C, pH 3, I = 10 A/dm^2	645 HV	–	–	[41]
Ni+ 14.6 vol % CNT	T = 40 °C, I = 0.04 A/cm^2	-	–	780	[42]
Ni + nano diamond	T = 60 °C, pH 3–4.5	701 HV	–	–	[43]
Ni + micro diamond	T = 60 °C, pH 3–4.5	550 HV	–	–	[43]

Table 2
Tribological properties: wear rate and COF of Ni-graphene, Ni-CNT and Ni-diamond coatings.

Coatings	EPD parameters	Testing	Wear rate	COF	References
Ni + 500 mg graphene	$T = 45$ °C, pH *4*, $I = 5$ A/dm^2	Sliding wear	8.5×10^{-4} mm^3/Nm	0.15	[44]
Ni + 500 mg graphene	$T = 45$ °C, pH 4, $I = 5$ A/dm^2	Sliding wear	10.1×10^{-4} mm^3/Nm	0.50	[44]
Ni-CNT	$T = 55$ °C, pH 3.8–4.2, $I = 3$ A/dm^2	Pin-on-disk	5.0×10^{-3} mg/m	0.15	[45]
Ni-CNT	$T = 55$ °C, pH 3.8, $I = 5$ A/dm^2	Ball-on-plate	27×10^{-15} m^3/m	–	[46]
Ni-CNT	$T = 55$ °C	Ball-on-plate	–	0.13	[47]
Ni + diamond	$T = 55$ °C, pH 3.8, $I = 2$ A/dm^2	Sliding wear	16×10^{-5} mm^3/Nm	–	[48]
Ni + nano-diamond	$T = 60$ °C, pH 3–4.5	Ball-on-disk	10×10^{-5} mm^3/Nm	–	[43]
Ni + micro-diamond	$T = 60$ °C, pH 3–4.5	Ball-on-disk	2×10^{-5} mm^3/Nm	–	[43]
Ni + nano-diamond	$T = 60$ °C, pH 3–4.5	Ball-on-disk	–	–	[49]

radio frequency components like tunable filters and nano transceivers [56]. Ni-doped CNT is widely used in the adsorption process of hydrogen storage. Mei-Yan et al. [57] and Seenithurai et al. [58] have also demonstrated the hydrogen storage behavior of Ni-doped SWCNT systems, which is a viable contender for fuel cell applications. By using the oil-gas analysis approach, a Ni-doped CNT gas sensor could efficiently identify gases in a transformer that were dissolved in oil. The energy of adsorption and charge transfer increased dramatically in the Ni/CNT system in comparison to the CNT structure alone. Based on this report, the electronic structures and sensitivities of Ni-doped CNT were effectively improved. and the electronic structures and the sensitivities of Ni-doped CNT had been efficiently improved. The sensitivity of adsorption for all three gases (C_2H_2, C_2H_4, and C_2H_6) with the Ni/CNT system is in the same order as observed in the case of the CNT system alone. The adsorption energies (in eV) and the charges (in e) were detected as C_2H_2 (−1.7412, 0.091) > C_2H_4 (−0.9246, 0.069) > C_2H_6 (−0.1994, 0.043). Ni-doped CNTs boosted the conductivity, catalytic activity, and surface-active sites of the CNTs, which was due to the unsaturation in coordination of the Ni ion surface atoms. The unique properties and characteristics of CNTs enable them to have a promising future in medicine. CNTs, being non-toxic, can move through membranes and carry therapeutic drugs to the target substrate. In some cases, CNTs enhance the solubility of drugs, resulting in great safety and efficiency [56].

3.3. Applications of diamond

Diamond particles have accelerated electro-catalytic activity, improved active sites, and amended electron transfer rate. Hence, it can be used in electroanalysis to enhance the reproducibility, selectivity, and sensitivity, of electrochemical and bio-electrochemical sensor probes [59]. Nowadays, Ni-diamond coated cutting tools have wide applications over typical cemented carbide cutting tools, for machining non-ferrous materials like fibre-reinforced polymers, copper alloys, aluminium-silicon alloys, ceramics and graphite due to their high hardness. Twist drills, inserts, square end mills and ball nose end mills are used as substrates for diamond-coated cutting tools. Comparison of the diamond coated cutting tool with the uncoated tool shows the high performance of diamond coated tool for the cutting of various work pieces like WC-Co, aluminium alloys, etc. For the better life of the tool, the diamond coating should be more than 10 μm. However, the increase in film thickness also causes problems related to the cutting performance due to the increased

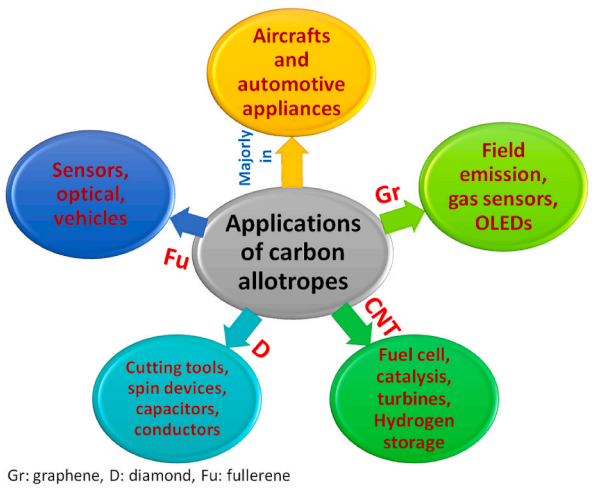

Fig. 5. Illustration of a variety of applications of carbon allotropes.

roundness of the cutting edge, roughness of coating and decreased strength [60]. Quantum activities in the solid state at the single spin level have gained much attention in the past few years. Diamond composites, having the ability to drive spin devices at room temperature, can be a potential material that offers opportunities to produce efficient quantum appliances for deployment from nanoscale to quantum computing [61]. Negatively charged nitrogen-vacancy (NV^-) colour centre in diamond has applications in quantum key distribution (which is the measure of strong attention for military and other commercial applications) and detection of magnetic fields [62]. The enhanced surface area, high stability as well as wide electrochemical potential of diamond particles can have potential uses in the disciplines of electrochemical capacitors or supercapacitors, dry sensitive solar cells, and lithium batteries [59]. Diamond honeycomb nanostructured-based electric double-layer capacitor has shown an electrochemical potential of 2.5 V and capacitance of 3910 μF cm^{-2} in aqueous electrolytes [63]. The diamond, when doped with boron, can act as a p-type semiconductor while the phosphorus doping results in n-type semiconductors with the bandgap 0.37 eV from the valence band maximum and 0.6 eV from the conduction band minimum [64,65]. However, a diamond can be used for photodetector with a bandgap of 5.5 eV and a sensitivity range of 185–250 nm, without doping, which has applications for the investigation of explosion and inflammation dynamics. Diamond particles, due to their large surface area and structural stability, can be used extensively as electrocatalysts in electrochemical reactions. Other applications of diamond incorporation include as a metal-free catalyst for steam-free dehydrogenation and oxidant [66]. The mechanical, thermal and optical properties of diamond are used in high-power IR lasers, optical windows and air-borne IR sensors. Therefore, it can be inference that the carbonaceous reinforcements have several applications in different fields. Fig. 5 presents a brief illustration of the diversity of applications of carbon allotropes.

4. Properties of Ni-carbonaceous coatings

4.1. Mechanical properties

The investigations of the mechanical properties (hardness, modulus, strength, fracture toughness, ductility) of material are the subject of high attention which involves a reaction to the applied load. Both theoretical and experimental observations indicated Ni with graphene, CNT and diamond as extraordinary metal matrix composites with high mechanical stiffness and strength [67,68]. The electrodeposition technique was used by Jiang et al. [38] to produce Ni-graphene coatings in their work. In order to complete this procedure, a temperature of 45 °C, a pH range of 3–4, and a current density of 0.1 A/cm^2 were all required. Graphene was present in the plating bath at different concentrations (0.1 and 0.2 g/l). An even surface was visible after scanning electron microscope examination. Surprisingly, the surface of the Ni-graphene coating showed a characteristic bulge-like pattern. The increased electrical conductivity of graphene was thought to be the cause of this phenomenon. Ni ions were reduced on the reinforced surface because of the incorporated reinforced particles' facilitation of electron transfer to the Ni matrix throughout the deposition process. As a result, certain bulging sections develop on the surface of the finished coating due to the deposition of Ni ions. Scherrer's equation was implemented to compute the average grain size, and it was discovered that pure Ni (35 nm) and 0.2 g/l Ni-graphene coatings both had lesser average grain sizes (16 nm and 18 nm, respectively). This was because pure Ni prevented the formation of grains for reduced Ni ions by improving the nucleation sites. The preferred nucleation occurred at (200) for all coatings but the addition of graphene platelets reduced the texture coefficient at the favoured orientation and enhanced at orientations of (111) and (220) due to the re-nucleation around the graphene platelets. $Ni(OH)_2$ is predicted to develop and be absorbed into the cathode surface as a result of reactions (1)–(4) taking place in the electroplating bath. This is expected to result in a drop in the textural coefficient at the desired orientation (200). However, Ni^{2+} and $Ni[B(OH)_4]^+$ cations can be engrossed on graphene platelets, protecting the Ni growth centers from the electrolyte's cations and preventing grains from growing any further. Renucleation is therefore rather likely, with (111) and (220) being the optimum nucleation orientations. Not all of the grains in the composite coatings will be impacted by the graphene platelets, and renucleation is more likely to occur around graphene platelets. This might account for the fact that all of the coatings' (200) orientations have the greatest texture coefficients, and the addition of graphene platelets has raised the coefficients of (111) and (220) orientations.

$$Ni + H_2O \rightarrow Ni(H_2O) \tag{1}$$

$$Ni(H_2O) \rightarrow Ni(OH)^+ + H^+ + 2e^- \tag{2}$$

$$Ni(OH)^+ + OH^- \rightarrow Ni(OH)_2 \tag{3}$$

$$B(OH)_3 + H_2O \leftrightarrow \left[B(OH)_4\right]^- + H^+ \tag{4}$$

The Vickers microhardness of the coatings was examined using a 100 g load for 20 s and observed an enhanced value of hardness (H) for 0.2 g/l Ni-graphene coatings (610 HV) compared to that of 0.1 g/l Ni-graphene coatings (580 HV) and pure Ni (270 HV) due to the small size and more effective strengthening effect. Ren et al. [39] created Ni-graphene coatings under specified parameters in their study, including a temperature of 50 °C, a period of 1–3 h, and a variable current density that varied from 0.15 to 4 A/dm2. The resultant coatings ranged in thickness from 5 to 10 μm. They performed nanoindentation experiments with an ideal force of 5 mN to measure the hardness and elastic modulus. Compared to pure Ni (with values of 3.9 GPa and 180 GPa, respectively), the Ni-graphene coating displayed significant improvements in hardness (4.7 GPa) and elastic modulus (240 GPa). This improvement is due to the powerful chemisorption enabled by the hybridization of graphene's p-orbitals with Ni's d-orbitals. This interaction between Ni and

graphene boosts carbon solubility within the Ni structure much more. Ni coatings mixed with graphite were also generated using the electrodeposition process to analyze the influence of different variables on the coating's topology. The parameters were optimized as time (10 min), current density (8–10 A/dm^2), and temperature (40 °C) [40]. The tensile strength was found to be higher for the coated samples than that of the bare steel substrate.

Researchers further continued their investigation of the mechanical characteristics of Ni-CNT coatings, which is also an important step toward providing structurally stable materials for airplanes, cars, and magnetic gadgets. Dai et al. [41] created a Ni-CNT coating with a bath temperature of 60 °C, a pH of 3, and a current density of 10 A/dm^2. Transmission electron microscopy (TEM) of the microstructure of the Ni-CNT coating is presented in Fig. 6. The CNTs distribution was homogenous in Ni-CNT composite coating (Fig. 6a) while Fig. 6b reveals the dispersion of single stick-shaped CNTs in the Ni matrix or dangling in the foil hole.

Further observations of mechanical properties of Ni-CNT coatings exhibited enhanced hardness and strength (σ) of Ni-CNT (hardness 645 HV, tensile strength 1475 MPa) coating than that of Ni coating (hardness 572 HV, tensile strength 1162 MPa) which was due to the fully dense coating prepared by electrodeposition without porosity and agglomeration of CNT in Ni matrix. Jeon et al. [42] electrodeposited Ni-CNT coatings using a Watts-type plating bath at 40 °C and 40 mA/cm^2 current density. The CNT content was varied from 0 to 10 g/l in the plating bath, and they observed a better vol. % of CNT (22.5 vol %) until 5 g/l of CNT concentration. The investigation of fracture toughness (KIC) revealed that with 14.6 vol % (2 g/l CNT), the toughness increases from 607 MPa to 780 MPa. However, at vol. % 22.5, the fracture toughness declines by up to 534 MPa due to the accumulation of CNTs in the Ni matrix. Moreover, Carpenter et al. [69] also performed co-deposition of Ni-CNT coatings under specific conditions: 55 °C, pH level of 3.8, and current density of 4 A/dm^2. They added varied quantities of CNT content (from 2 to 20 g/l) to the plating bath and saw a significant increase in the volume percentage of CNTs (to 3.9 vol %) within the Ni-CNT coating. This increased CNT proportion was accomplished by introducing up to 20 g/l of CNTs into the bath. The increased hardness (measured at 550 kgf/mm^2) was attributable to the improvement of grain size (dropping from 72 to 45 nm) in the Ni-CNT coating, which demonstrated a clear association with the rising amounts of CNT material within the bath (varying from 2 to 20 g/l).

Additionally, Gou et al. [70] explored the effect of surfactants on electrodeposited Ni-CNT coatings, especially sodium dodecyl sulfate (SDS) and hexadecyltrimethylammonium bromide (CTAB). This experiment was conducted at a temperature of 54 °C, a pH of 4, and a current density of 4 A/dm^2. The addition of SDS resulted in a decrease in CNT content inside the Ni matrix, but CTAB increased CNT insertion. The anionic character of the functional unit in SDS became absorbed onto the CNT surface, causing the CNTs to be opposed by the cathode. CTAB, on the other hand, positively charged the CNT surface with cations, enhancing its binding to the cathode. The degree of hardness demonstrated a diverging response in comparison to the CNT content. When the CNT content was elevated to 0.3 g/l with the addition of SDS surfactant, the hardness increased to 280 HV. However, the addition of CTAB had a negative impact, lowering the hardness of the Ni-CNT coating to as low as 40 HV. The basic root of this discrepancy is due to the opposing mechanisms at work. The anionic character of CNT surfaces (due to SDS) makes them susceptible to attraction by Ni^{2+} ions, enhancing the Ni-CNT composite's strengthening process. The cationic character of CNT surfaces (due to CTAB) on the other hand, hampers the composite's stiffening process.

Wang et al. [43] compared electrodeposited microcrystalline (m-Ni/diamond) and nanocrystalline diamond (n-Ni/diamond) particle systems inside a Ni matrix. The experiments were executed at 45 °C and a pH range of 3–4.5. The analysis found that the nano-Ni-diamond coating scheme excelled over the micro-Ni-diamond coating scheme in terms of microhardness (measuring 701 kg/mm^2). The dispersion of the reinforcing process was responsible for the increase in microhardness. Table 1 summarizes the mechanical parameters of nickel-carbonaceous composite coatings for simple inspection, allowing readers to make quick assessments.

4.2. Tribological properties

The study of friction, lubrication and wear is of enormous practical importance for the applications of the material in aircraft, vehicles, electromagnetic, sensors, capacitors etc [44]. So, for this purpose, Hamid et al. [71] electrodeposited Ni coating at a temperature 45 °C and pH 3.6 followed by the heat treatment to 520 °C for 10 h in an argon atmosphere. Pin-on-disk tribometer was used with a normal load of 2 N to observe the friction coefficient of the coating. However, the microswitch testing was performed to check

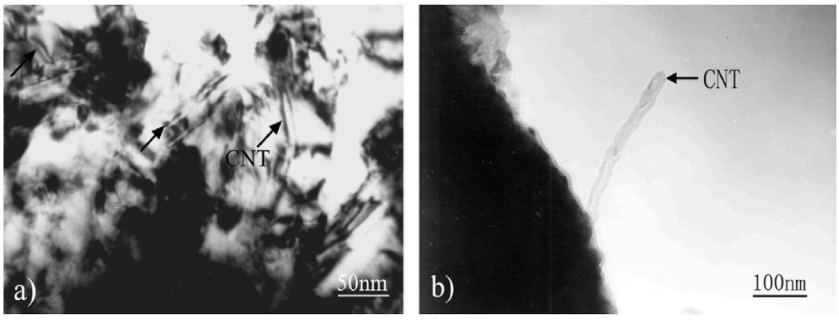

Fig. 6. TEM images of Ni-CNT composite: (a) CNTs distribution in Ni matrix and (b) CNT dangled in the foil hole. Reproduced with permission from ref. [41].

the adhesion and fracture characteristics of the coating using a Rockwell indenter of 100 μm tip radius. The progressive load was used from 0.1 N to 30 N with a loading rate of 60 N/mm. The friction-of-coefficient (COF) was observed to be 0.70 while there was no sign of de-cohesion or cracking of Ni coating after microscratch testing with penetration depth of 6.6 μm. Further, for Ni-carbonaceous coatings, Algul et al. [44] assessed the tribological behavior of Ni-graphene coating using sliding wear with 3 different sliding speeds of 50 mms^{-1}, 100 mms^{-1} and 150 mms^{-1}, keeping constant normal load 1.0 N. The wear rate (from 9.2×10^{-4} mm^3/Nm to 8.6×10^{-4} mm^3/Nm) and COF (from 0.35 to 0.10) were decreased linearly with increase in the sliding speed due to the decrease in running time with increase in the sliding speed, resulting in an increase of hardness of coating surface with the formation of oxide which reduces the wear rate and friction coefficient. Nonetheless, the wear rate and COF were also evaluated with the increasing content of graphene in the plating bath from 100 mg/l to 500 mg/l and it was reported that as the concentration of graphene increases, the wear rate (from 10.1×10^{-4} mm^3/Nm to 8.5×10^{-4} mm^3/Nm) and COF (from 0.50 to 0.15) decrease due to the lubrication effect of graphene which reduces the plastic deformation by smearing. However, Dai et al. [41] studied sliding wear of Ni-CNT coatings with a load of 30 N for 5 min and observed 1.8 mg of wear loss for Ni-CNT coating without the cracks and plastic deformation of the surface after the wear test while pure Ni coating shows 3.1 mg of wear loss with significant microcracks, plastic deformation and fragmentation. CNT in Ni matrix reduces the direct contact between the coating and counter body as well as the lubrication phenomenon can improve the wear resistance of Ni-CNT coating. Tu et al. [45] fabricated Ni-CNT coatings at 55 °C temperature, pH 3.8–4.2 and 3 A/dm^2 current density and observed friction and wear performance of coating applying pin-on-disk tribometer with load 12 N–150 N and observed an enhanced coefficient-of-friction (from 0.15 to 0.20) and wear rate (increased from 5×10^{-3} mg/m to 20×10^{-3} mg/m) was monitored with increasing the load because increased load causes spalling and cracking of the coatings. Moreover, Borkar et al. [72] fabricated Ni-CNT coatings at 25 °C temperature, pH 4 and 5 A/dm^2 current density. The wear test was performed using a ball-on-disk arrangement with a load of 7 N and an average speed of 150 rev/min at 4-min intervals. The pure Ni coating revealed nearly linear wear loss with time. Improved wear resistance was observed by Ni-CNT coating with less weight loss (0.5 mg) and plastic deformation compared to that of Ni coating (1.7 mg). Carpenter et al. [46] engineered Ni-CNT coatings at 55 °C, pH 3.8, 20 % duty cycle, and 5 A/dm^2 current density. The wear testing was performed with a ball-on-plate wear tester using a varying normal load from 0.5 N to 10 N, an amplitude of motion of 10 mm, a sliding speed of 40 mm, and a frequency of 2 Hz. Initially, wear rate enhancements were observed with increasing normal load, in which Ni-CNT coating showed a lesser wear rate (27×10^{-15} m^3/m) than Ni coating (127×10^{-15} m^3/m) due to the lubrication of bearing effect of CNTs between the coating and counter body. Arai et al. [47] also electrodeposited Ni-CNT coatings using a Watts bath at 25 °C. Tribological characteristics were examined using a ball-on-plate wear tester at a normal load of 1 N, 10 mm friction stroke, 40 mm/s sliding speed, and 2600 cycles. The COF was measured during the wear test, and it was monitored that Ni-CNT coating exhibited less COF (0.13) and fluctuations with increasing the number of cycles than that of pure Ni coating (0.33), which showed a high magnitude of fluctuations. In Ni-CNT coatings, CNTs show intrinsic self-lubrication at the tribological surface, which prevents wear loss during testing and increases the wear resistance of Ni-CNT coatings.

Further, Huang et al. [48] also created Ni-diamond coatings using EPD technology to examine the tribological properties of Ni-diamond coatings. The temperature was set to 55 °C, the pH was set to 3.8, and the current density was set to 2 A/dm^2. Following that, an anti-wear experiment was carried out with a weight of 2 N and a sliding speed of 0.1 m/s. Fig. 7 depicts the results, indicating that pure Ni (shown in Fig. 7a) has a smoother surface with no identifiable characteristics. Fig. 7b, on the other hand, shows diamond particles that are equally dispersed throughout the surface. Notably, the diamond coating's wear rate (measured at 16×10^{-5} mm^3/Nm) was found to be lower than that of pure Ni (measured at 39×10^{-5} mm^3/Nm). This enhancement was due to the dispersion-strengthening result induced by the introduction of diamond particles.

Additionally, Wang et al. [43] examined electrodeposited microcrystalline (m-Ni/diamond) and nanocrystalline diamond (n-Ni/diamond) particles in Ni matrix and discovered that nano Ni-diamond coating system had higher resistance to wear than micro-Ni-diamond coating system. The wear rate in n-Ni/diamond coating is greater (10×10^{-5} mm^3/Nm) than in pure m-Ni coating (2×10^{-5} mm^3/Nm), which is related to the dragging out of agglomerated diamond particles from the Ni matrix. The reduction of crack propagation along with the improvement in the toughness by the addition of nanodiamonds in nickel matrix was reported by Yazdani et al. [49]. The reduction in sp^3 disordered atoms and diamond ration was attributed to the crack propagation blocking. The summarized research is given in Table 2.

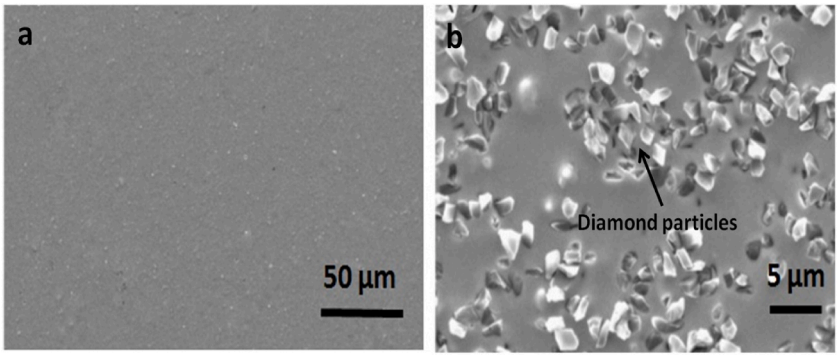

Fig. 7. SEM images of (a) pure Ni coating and (b) Ni-diamond coating. Reproduced with permission from ref [48].

4.3. Electrochemical properties

The gradual destruction of material by chemical reactions with the environment can impact the material's properties like mechanical strength and appearance. For the protection of materials from corrosion, a coating of adherent material is fabricated on the exposed surface of the material. There are several types of corrosion that occur on the metallic surface, including pitting, crevice corrosion, intergranular corrosion, galvanic corrosion, etc. To preserve the metal's surface, Jiang et al. [38] investigated the electrochemical characteristics of Ni and Ni-graphene coatings with variable graphene content (0.1 g/l and 0.2 g/l) in a 3.5 % NaCl solution using a potential sweep rate of 1.0 mV/s. However, resistance was measured at frequencies ranging from 0.01 Hz to 10 kHz. Enhanced corrosion resistance was observed for 0.2 g/l Ni-graphene coating (Icorr 0.398 μA/cm^2) in comparison to 0.1 g/l Ni-graphene (Icorr 3.02 μA/cm^2) as well as pure Ni coating (Icorr 19.1 μA/cm^2).

Additionally, Benigna et al. [73] carried out the deposition of Ni-graphene coatings at 45 °C, pH 4, and 4 A/dm^2 of current density. Using a voltammetric technique in a 0.5 M NaCl solution, the Ni-graphene coating's anti-corrosion property was measured. Three different graphene quantities (0.3, 0.5, and 1 g/dm^3) were added to the bath. According to the findings, corrosion resistance and graphene concentration are directly correlated. Notably, the corrosion resistance improved correspondingly with the increase in graphene content. This behavior was demonstrated by the linear decrease in corrosion rate, which was measured at 1.48 10-3 mm/year for a 1 g/dm^3 concentration of graphene. The ability of graphene to diminish the exposure of the metallic surface to corrosive conditions was linked to the improvement in resisting corrosion. The variation of graphene with nickel coatings was reported and studied for electrochemical effects by Akbarpour et al. [74]. They observed a reduced corrosion rate with the addition of graphene up to an optimum concentration; after that content, the corrosion resistance started decreasing.

Guo et al. [75] investigated the influence of current density on the corrosion of a Ni-CNT coating in a 3.5 % NaCl solution. The frequency range for the electrochemical impedance measurements was set at 100 kHz to 0.01 Hz from the open circuit potential. The carbon content increases at 8 A/dm^2 current density, while the resistance to corrosion upgrades (polarization resistance 5.5 × 104 Ω cm^2) at the same current density and starts declining as current density increases above 8 A/dm2 (polarization resistance 4.2 × 104 Ω cm^2). Additionally, the effect of surfactants (SDS and CTAB) on the corrosion resistance of Ni-CNT coatings was also demonstrated by Guo et al. [70] The use of SDS surfactant improves corrosion inhibition with an increased CNT concentration. On the other hand, the presence of CTAB reduces the coating's ability to prevent corrosion. This can be related to the antagonistic nature of the cationic surface of CNTs (due to CTAB), which weakens the strengthening mechanism of the Ni-CNT composite, and the anionic surface of CNTs (arrives from SDS), which increases adhesion by Ni^{2+} ions. Moreover, enhancing the Ni-B alloy structure by reinforcing it with TiC particles and electrodepositing it onto AISI 304 stainless steel was studied by Ersin et al. [76]. AISI 304, which is widely used throughout the globe, was chosen for its low cost, mechanical strength, corrosion resistance, and weldability. The research effort investigates how TiC particle and trimethylamine borane (TMAB) bath concentration, as well as current density during electrodeposition, influence Ni-B/TiC nanocomposite coating [76]. Additionally, it was observed that nanocrystalline Ni-tungsten (W) coatings, with their better hardness, corrosion resistance, and thermal stability, may be able to substitute hexavalent hard chrome [77]. Notably, the tungsten (W) concentration and dispersion influence the corrosion behavior of the coating [78]. Argaaraz et al. found that Ni-W had better corrosion resistance than bare carbon steel in a phosphate-borate buffer system [79].

4.4. Magnetic properties

Numerous magnetic devices (actuators, sensors, memorizers, magnetic recording heads, spintronics) that are widely used in the form of micro or nanofilms rely heavily on the magnetism of Ni and Ni-based carbonaceous coatings. Nasirpouri et al. [80] used a temperature of 55 °C, a pH of 4.6, and various current densities between 2 and 8 A/dm^2 to electrodeposit Ni-CNT coatings. The coating's CNT content increased until a current density of 4 A/dm^2, when it peaked at 5.1 vol %, and then began to fall to 3.8 vol %. Magnetic hysteresis loops were captured in various combinations to look at the magnetic properties of the coatings.

The change in microstructure and domain wall movement at the Ni-CNT junction, which was attributed to the orientation dependency of the magnetization reversal process, led to distinct values of coercivity and squareness being recorded from various perspectives. The coercivity was observed for 5.1 vol % CNT to be 107 Oe for in-plane and 132 Oe for out-of-plane orientations due to the decrease in grain size (25.9 nm). However, different CNT concentrations lead to a change in the crystallographic texture of the coatings, which accounts for different squareness values (0.29 for in-plane and 0.09 for out-of-plane). As coating technologies continue to evolve, different engineering criteria must be met. In this regard, nanostructured Ni alloy coatings have become more and more popular in a wide range of engineering applications. Particularly when juxtaposed with conventional coatings with a rough grain structure, nanostructured coatings featuring crystal grains smaller than 100 nm present entirely distinct features [81]. For example, a nickel-iron titanium carbide (Ni–Fe–TiC) nanocomposite onto St14 low-carbon steel using pulse electrodeposition, decreased corrosion current density compared to a Ni–Fe coating [82]. On the other hand, the Ni-Fe alloy coating is utilized to reduce manufacturing expenses while simultaneously providing soft magnetic characteristics, strong conductivity of electricity, durability against corrosion, and specific photonic qualities [83].

5. Conclusions and future prospects

The review of current research emphasizes the importance of electrodeposited Ni-carbonaceous coatings for a variety of purposes. The incorporation of various kinds of carbonaceous reinforcements, on the other hand, offers the potential to improve surface qualities such as hardness and various corrosion resistance. The mechanical stability, wear resistance, and corrosion resistance of the exposed

surface can be significantly increased by introducing carbonaceous reinforcements into the Ni matrix. This enhancement is attributed to techniques such as dispersion strengthening, lubricating effects, and grain improvement, which are enabled by the incorporation of elements such as diamond, carbon nanotubes (CNTs), and graphene into the Ni matrix. However, the literature gap can be sealed by the evolution of missing characterizations for the aforementioned coatings. Further work is required in the fields of multi-length tribological characterizations, corrosion studies, and magnetism studies to develop high-strength Ni-carbonaceous composites for aerospace, automotive, and magnetic appliances. The protection of vehicles and aircraft from corrosion and wear without major maintenance to encounter stringent environmental, safety, and performance requirements is the fundamental factor for the stimulation of present research in the field of Ni-carbonaceous composite coatings. Although significant progress has been made in understanding the deposition parameters, the effect of parameters on the properties of the coatings, and the microstructure and phase characterizations of Ni-diamond, Ni-CNT, and Ni-graphene coatings, electrochemical observation for Ni-graphene and Ni-CNT coatings is present to a minor extent (missing for Ni-diamond), while magnetism and multi-length tribological studies for Ni-graphene and Ni-diamond coatings are completely missing in the literature. Fullerene is an important allotrope of carbon and can be utilized for various applications including biomedical, conductors, water purification and catalytic activities. The studies related to Ni-fullerene composite coatings have not been explored by the researchers yet and can be a remarkable work in future. Therefore, this review report is envisioned to be a comprehensive, accessible, and critical review for the benefit of chemical, material, and physicist societies that are working on coatings related to nickel, carbonaceous materials, and composites for a broad area of applications, including aerospace, automotive, and other industries. The intended demand for automotive and aerospace materials makes carbon nanoallotropes and metallic coatings one of the preferred choices for research and development. It is firmly believed that this report will attract a broad scientific community of chemical, material, and physical researchers.

CRediT authorship contribution statement

Shikha Awasthi: Writing – review & editing. **Suranjan De:** Writing – original draft. **Sarvesh Kumar Pandey:** Writing – original draft.

Declaration of competing interest

The authors declare that they have no known competing financial interests or personal relationships that could have appeared to influence the work reported in this paper.

Acknowledgements

Authors acknowledges the Department of Chemistry, Manipal University Jaipur.

References

[1] P. Simon, Y. Gogotsi, Materials for electrochemical capacitors, Nat. Mater. 7 (2008) 845–854.
[2] M.E. McRae, U.S. Geological Survey, Mineral Commodity Summaries: Nickel, 2016.
[3] T.M. Pollock, Alloy design for aircraft engines, Nat. Mater. 15 (2016) 809–815.
[4] S. Wollschlaeger, Enhanced Methods for Nickel Recovery from Low-Grade Ores and Bleed Streams, 2017.
[5] S. Barnett, Magazine on Nickel, The Nickel Institute, Canada 2007.
[6] E. Ünal, A. Yaşar, İ.H. Karahan, Effect of trimethylamine borane (TMAB) bath concentration on electrodeposited Ni–B/TiC nanocomposite coatings, Ceram. Int. 49 (2023) 25516–25529.
[7] B. Li, W. Zhang, Y. Huan, J. Dong, Synthesis and characterization of Ni-B/Al2O3 nanocomposite coating by electrodeposition using trimethylamine borane as boron precursor, Surf. Coat. Technol. 337 (2018) 186–197.
[8] B. Li, W. Zhang, T. Mei, Y. Miao, Fabrication of Ni–B/TiC–Y2O3 nanocomposites by one-step electrodeposition at different duty cycle and evaluation of structural, surface and performance as protective coating, J. Alloys Compd. 823 (2020) 153888.
[9] M.S. Safavi, A. Rasooli, The positive contribution of Cr2O3 reinforcing nanoparticles to enhanced corrosion and tribomechanical performance of Ni–Mo alloy layers electrodeposited from a citrate-sulfate bath, J. Mater. Res. Technol. 28 (2024) 865–878.
[10] M. Kartal, I. Buyukbayram, A. Alp, H. Akbulut, Production of pulse electrodeposited Ni-TiC nanocomposite coatings, Mater Today Proc 4 (2017) 6982–6989.
[11] M. Karbasi, N. Yazdian, A. Vahidian, Development of electro-co-deposited Ni–TiC nano-particle reinforced nanocomposite coatings, Surf. Coat. Technol. 207 (2012) 587–593.
[12] M.İ. Coşkun, İ.H. Karahan, Modeling corrosion performance of the hydroxyapatite coated CoCrMo biomaterial alloys, J. Alloys Compd. 745 (2018) 840–848.
[13] H.K. Ghritlahre, R.K. Prasad, Application of ANN technique to predict the performance of solar collector systems - a review, Renew. Sustain. Energy Rev. 84 (2018) 75–88.
[14] X. Li, Y. Zhu, G. Xiao, Application of artificial neural networks to predict sliding wear resistance of Ni–TiN nanocomposite coatings deposited by pulse electrodeposition, Ceram. Int. 40 (2014) 11767–11772.
[15] D.E. Calhane, A.I. Gammage, A study of the causes of impure nickel plate with special reference to the iron, J. Am. Chem. Soc. 29 (1907) 1268–1274.
[16] G.A. DiBari, Nickel electroplating applications and trends, Plating Surf Finish 83 (1996) 10–14.
[17] R. Ambat, W. Zhou, Electroless nickel-plating on AZ91D magnesium alloy: effect of substrate microstructure and plating parameters, Surf. Coat. Technol. 179 (2004) 124–134.
[18] T. Maruyama, T. Tago, Nickel thin films prepared by chemical vapour deposition from nickel acetylacetonate, J. Mater. Sci. 28 (1993) 5345–5348.
[19] A. Chaparro, W. Arnulfo, E. Vera, Electrodeposition of nickel plates on copper substrates using PC y PRC, Rev. Mater. 12 (2007) 583–588.
[20] H.M. Alojali, K.Y. Benyounis, Advances in Tool Wear in Turning Process. Reference Module in Materials Science and Materials Engineering, Elsevier, 2016.
[21] D.W. Hoeppner, L. Grimes, A. Hoeppner, J. Ledesma, T. Mills, A. Shah, Corrosion and fretting as critical aviation safety issues,", in: Proceedings of the 18th Symposium on the International Committee of Aeronautical Fatigue, 1995.
[22] S.C. Tung, M.L. McMillan, Automotive tribology overview of current advances and challenges for the future, Tribol. Int. 37 (2004) 517–536.
[23] G. Pal, S. Kumar, Modeling of carbon nanotubes and carbon nanotube-polymer composites, Prog. Aero. Sci. 80 (2016) 33–58.

[24] D.R. Rolison, J.W. Long, J.C. Lytle, A.E. Fischer, C.P. Rhodes, T.M. McEvoy, et al., Multifunctional 3D nanoarchitectures for energy storage and conversion, Chem. Soc. Rev. 38 (2009) 226–252.
[25] N. Deprez, D.S. McLachlan, The analysis of the electrical conductivity of graphite conductivity of graphite powders during compaction, J. Phys. D Appl. Phys. 21 (2000) 101–107.
[26] X. Wang, L. Zhi, K. Müllen, Transparent, conductive graphene electrodes for dye-sensitized solar cells, Nano Lett. 8 (2007) 323–327.
[27] S. Iijima, Helical microtubules of graphitic carbon, Nature 350 (1991) 627–628.
[28] Q. Shu, J. Wei, K. Wang, H. Zhu, Z. Li, Y. Jia, et al., Hybrid heterojunction and photoelectrochemistry solar cell based on silicon nanowires and double-walled carbon nanotubes, Nano Lett. 9 (2009) 4338–4342.
[29] D.M. Gruen, O.A. Shenderova, AYa Vul, Synthesis, Properties and Applications of Ultrananocrystalline Diamond, Published by Springer, St. Petersburg, Russia, 2004.
[30] G. Lalwani, B. Sitharaman, Multifunctional fullerene- and metallofullerene-based nanobiomaterials, Nano Life 3 (2013) 1342003–1342025.
[31] H. Abi-akar, C. Riley, G. Maybee, Electrocodeposition of nickel - diamond and cobalt - chromium carbide in low gravity, Chem. Mater. 4756 (1996) 2601–2610.
[32] A. Malesevic, R. Kemps, A. Vanhulsel, M.P. Chowdhury, A. Volodin, C. Van Haesendonck, Field emission from vertically aligned few-layer graphene, J. Appl. Phys. 104 (2008) 1–6.
[33] J. Molina, Graphene-based fabrics and their applications: a review, RSC Adv. 6 (2016) 68261–68291.
[34] F. Schedin, A. Geim, S.V. Morozov, E.W. Hill, P. Blake, M.I. Katsnelson, et al., Detection of individual gas molecules adsorbed on graphene, Nat. Mater. 6 (2007) 652–655.
[35] K.S. Novoselov, A.K. Geim, S.V. Morozov, D. Jiang, Y. Zhang, S.V. Dubonos, et al., Electric field effect in atomically thin carbon films, Science (1979) 306 (2004) 20–23.
[36] A.G. Basutkar, A. Kolekar, A review on properties and applications of ceramic matrix composites, Journal of Material Science and Mechanical Engineering 2 (2015) 28–30.
[37] J.C. Meyer, A.K. Geim, M.I. Katsnelson, K.S. Novoselov, T.J. Booth, S. Roth, The structure of suspended graphene sheets, Nature 446 (2007) 60–63.
[38] K. Jiang, J. Li, J. Liu, Electrochemical codeposition of graphene platelets and nickel for improved corrosion resistant properties, RSC Adv. 4 (2014) 36245–36252.
[39] Z. Ren, N. Meng, K. Shehzad, Y. Xu, S. Qu, B. Yu, et al., Mechanical properties of nickel-graphene composites synthesized by electrochemical deposition, Nanotechnology 26 (2015) 65706–65714.
[40] P.K. Rai, A. Gupta, Investigation of surface characteristics and effect of electrodeposition parameters on nickel-based composite coating, Mater Today Proc 44 (2021) 1079–1085, https://doi.org/10.1016/j.matpr.2020.11.182.
[41] P.Q. Dai, W.C. Xu, Q.Y. Huang, Mechanical properties and microstructure of nanocrystalline nickel-carbon nanotube composites produced by electrodeposition, Mater. Sci. Eng. 483–484 (2008) 172–174.
[42] Y.S. Jeon, J.Y. Byun, T.S. Oh, Electrodeposition and mechanical properties of Ni-carbon nanotube nanocomposite coatings, J. Phys. Chem. Solid. 69 (2008) 1391–1394.
[43] L. Wang, Y. Gao, Q. Xue, H. Liu, T. Xu, Effects of nano-diamond particles on the structure and tribological property of Ni-matrix nanocomposite coatings, Mater. Sci. Eng. 390 (2005) 313–318.
[44] H. Algul, M. Tokur, S. Ozcan, M. Uysal, T. Cetinkaya, H. Akbulut, et al., The effect of graphene content and sliding speed on the wear mechanism of nickel-graphene nanocomposites, Appl. Surf. Sci. 359 (2015) 340–348.
[45] J.P. Tu, L.P. Zhu, W. Chen, X. Zhao, F. Liu, X. Zhang, Preparation of Ni-CNT composite coatings on Al substrate and its friction and wear behavior, Trans. Nonferrous Metals Soc. China 14 (2004) 880–884.
[46] C.R. Carpenter, P.H. Shipway, Y. Zhu, Electrodeposition of nickel-carbon nanotube nanocomposite coatings for enhanced wear resistance, Wear 271 (2011) 2100–2105.
[47] S. Arai, A. Fujimori, M. Murai, M. Endo, Excellent solid lubrication of electrodeposited nickel-multiwalled carbon nanotube composite films, Mater. Lett. 62 (2008) 3545–3548.
[48] W. Huang, Y. Zhao, X. Wang, Preparing a high-particle-content Ni/diamond composite coating with strong abrasive ability, Surf. Coat. Technol. 235 (2015) 489–494.
[49] S. Yazdani, M. Mesbah, V. Dupont, V. Vitry, Microstructure, wear and crack propagation evolution of electrodeposited nickel-nano diamond composite coatings: molecular dynamic modeling and experimental study, Surf. Coat. Technol. 462 (2023) 129500, https://doi.org/10.1016/j.surfcoat.2023.129500.
[50] Y.W. Jin, J.E. Jung, Y.J. Park, J.H. Choi, D.S. Jung, H.W. Lee, et al., Triode-type field emission array using carbon nanotubes and a conducting polymer composite prepared by electrochemical polymerization, J. Appl. Phys. 92 (2002) 1065–1068.
[51] G. Girishkumar, M. Rettker, R. Underhile, D. Binz, K. Vinodgopal, P. Mcginn, et al., Single-wall carbon nanotube-based proton exchange membrane assembly for hydrogen fuel cells, Langmuir (2005) 8487–8494.
[52] C.Y. Lee, H.M. Tsai, H.J. Chuang, S.Y. Li, P. Lin, T.Y. Tseng, Characteristics and electrochemical performance of supercapacitors with manganese oxide-carbon nanotube nanocomposite electrodes, J. Electrochem. Soc. 152 (2005) A716–A720.
[53] M. Ajayan, O. Zhou, Applications of Carbon Nanotubes," Carbon Nanotubes''Top. Appl. Phys, Springer-Verlag Berlin Heidelb, 2001.
[54] Y. Kong, T. Qiu, J. Qiu, Fabrication of novel micro-nano carbonous composites based on self-made hollow activated carbon fibers, Appl. Surf. Sci. 265 (2013) 352–357.
[55] K.-W. Ng, W.-H. Lam, S. Pichiah, A review on potential applications of carbon nanotubes in marine current turbines, Renew. Sustain. Energy Rev. 28 (2013) 331–339.
[56] S.W. Lee, E.E.B. Campbell, Nanoelectromechanical devices with carbon nanotubes, Curr. Appl. Phys. 13 (2013) 1844–1859.
[57] N. Mei-Yan, W. Xian-Long, Z. Zhi, Interaction of hydrogen molecules on Ni-doped single-walled carbon nanotube, Chin. Phys. B 18 (2009) 357–362.
[58] S. Seenithurai, R. Kodi Pandyan, S. Vinodh Kumar, M. Mahendran, H2 adsorption in Ni and passivated Ni doped 4 ?? single walled carbon nanotube, Int. J. Hydrogen Energy 38 (2013) 7376–7381.
[59] N. Yang, J.S. Foord, X. Jiang, Diamond electrochemistry at the nanoscale: a review, Carbon N Y 99 (2016) 90–110.
[60] K. Kanda, S. Takehana, S. Yoshida, R. Watanabe, S. Takano, H. Ando, et al., Application of diamond-coated cutting tools, Surf. Coat. Technol. 73 (1995) 115–120.
[61] M.L. Markham, J.M. Dodson, G.A. Scarsbrook, D.J. Twitchen, G. Balasubramanian, F. Jelezko, et al., CVD diamond for spintronics, Diam. Relat. Mater. 20 (2011) 134–139.
[62] G. Balasubramanian, P. Neumann, D. Twitchen, M. Markham, R. Kolesov, N. Mizuochi, et al., Ultralong spin coherence time in isotopically engineered diamond, Nat. Mater. 8 (2009) 383–387.
[63] K. Honda, T.N. Rao, D.a. Tryk, A. Fujishima, M. Watanabe, K. Yasui, et al., Electrochemical characterization of the nanoporous honeycomb diamond electrode as an electrical double-layer capacitor, J. Electrochem. Soc. 147 (2000) 659–664.
[64] H. Okazaki, R. Yoshida, T. Muro, T. Nakamura, T. Wakita, Y. Muraoka, et al., Multiple phosphorus chemical sites in heavily phosphorus-doped diamond, Appl. Phys. Lett. 98 (2011) 082107. –10.
[65] E. Gheeraert, S. Koizumi, T. Teraji, H. Kanda, M. Nesladek, Electronic states of phosphorus in diamond, Diam. Relat. Mater. 9 (2000) 948–951.
[66] Z. Zhao, Y. Dai, Nanodiamond/carbon nitride hybrid nanoarchitecture as an efficient metal-free catalyst for oxidant- and steam-free dehydrogenation, J Mater Chem A Mater 2 (2014) 13442–13451.
[67] S. Inoue, Y. Matsumura, Molecular dynamics simulation of metal coating on single-walled carbon nanotube, Chem. Phys. Lett. 464 (2008) 160–165.
[68] S. Inoue, Y. Matsumura, Influence of metal coating on single-walled carbon nanotube: molecular dynamics approach to determine tensile strength, Chem. Phys. Lett. 469 (2009) 125–129.

[69] C.R. Carpenter, P.H. Shipway, Y. Zhu, The influence of CNT co-deposition on electrodeposit grain size and hardness, Surf. Coat. Technol. 205 (2011) 5059–5063.
[70] C. Guo, Y. Zuo, X. Zhao, J. Zhao, J. Xiong, Effects of surfactants on electrodeposition of nickel-carbon nanotubes composite coatings, Surf. Coat. Technol. 202 (2008) 3385–3390.
[71] A. Ul-Hamid, A. Quddus, F.K. Al-Yousef, A.I. Mohammed, H. Saricimen, L.M. Al-Hadhrami, Microstructure and surface mechanical properties of electrodeposited Ni coating on Al 2014 alloy, Surf. Coat. Technol. 205 (2010) 2023–2030.
[72] T. Borkar, S. Harimkar, Microstructure and wear behaviour of pulse electrodeposited Ni-CNT composite coatings, Surf. Eng. 27 (2011) 524–530.
[73] B. Szeptycka, A. Gajewska-Midzialek, T. Babul, Electrodeposition and corrosion resistance of Ni-graphene composite coatings, J. Mater. Eng. Perform. 25 (2016) 3134–3138.
[74] M.R. Akbarpour, F. Gharibi Asl, H. Rashedi, Pulse-reverse electrodeposition of Ni-Co/graphene composite films with high hardness and electrochemical behaviour, Diam. Relat. Mater. 133 (2023) 109720, https://doi.org/10.1016/j.diamond.2023.109720.
[75] C. Guo, Y. Zuo, X. Zhao, J. Zhao, J. Xiong, The effects of electrodeposition current density on properties of Ni-CNTs composite coatings, Surf. Coat. Technol. 202 (2008) 3246–3250.
[76] E. Ünal, A. Yaşar, İ.H. Karahan, Estimation of microhardness and crystal grain size values of electrodeposited Ni-B/TiC nanocomposite coatings by artificial neural networks (ANN) method, J. Alloys Compd. 966 (2023) 171677.
[77] L. Elias, A.C. Hegde, Effect of magnetic field on corrosion protection efficacy of Ni-W alloy coatings, J. Alloys Compd. 712 (2017) 618–626.
[78] L. Elias, A. Chitharanjan Hegde, Electrodeposition of laminar coatings of Ni–W alloy and their corrosion behaviour, Surf. Coat. Technol. 283 (2015) 61–69.
[79] M.P.Q. Argañaraz, S.B. Ribotta, M.E. Folquer, L.M. Gassa, G. Benítez, M.E. Vela, et al., Ni–W coatings electrodeposited on carbon steel: chemical composition, mechanical properties and corrosion resistance, Electrochim. Acta 56 (2011) 5898–5903.
[80] F. Nasirpouri, F. Daneshvar-Fattah, A. Samardak, E. Sukovatitsina, A. Ognev, L. Chebotkevich, Magnetic properties of electrodeposited nickel-multiwall carbon nanotube composite films, IEEE Trans. Magn. 51 (2015) 1–4.
[81] M.A. Alam, H.H. Ya, M. Azeem, P Bin Hussain, M.S. bin Salit, R. Khan, et al., Modelling and optimisation of hardness behaviour of sintered Al/SiC composites using RSM and ANN: a comparative study, J. Mater. Res. Technol. 9 (2020) 14036–14050.
[82] M. Ganji, H. Yousefnia, Z.S. Seyedraoufi, Y. Shajari, The corrosion behavior of Ni–Fe and Ni–Fe–TiC nanoparticles deposited using pulse electrodeposition on low-carbon steel, Journal of the Australian Ceramic Society 58 (2022) 1283–1295.
[83] Á. Llavona, L. Pérez, M.C. Sánchez, V. de Manuel, Enhancement of anomalous codeposition in the synthesis of Fe–Ni alloys in nanopores, Electrochim. Acta 106 (2013) 392–397.